Common envelope evolution in born-again planetary nebulae – Shaping the H-deficient ejecta of A 30

J. B. Rodríguez-González [ORCID],[1]★ E. Santamaría [ORCID],[2,3] J. A. Toalá [ORCID],[1]† M. A. Guerrero [ORCID],[4] B. Montoro-Molina,[4] G. Rubio [ORCID],[2,3] D. Tafoya,[5] Y.-H. Chu,[6] G. Ramos-Larios [ORCID][2,3] and L. Sabin [ORCID][7]

[1]*Instituto de Radioastronomía y Astrofísica, UNAM, Antigua Carretera a Pátzcuaro 8701, Ex-Hda. San José de la Huerta, Morelia 58089, Mich., Mexico*
[2]*CUCEI, Universidad de Guadalajara, Blvd. Marcelino García Barragán 1421, 44430 Guadalajara, Jalisco, Mexico*
[3]*Instituto de Astronomía y Meteorología, Depto. de Física, CUCEI, Av. Vallarta 2602, 44130 Guadalajara, Jalisco, Mexico*
[4]*Instituto de Astrofísica de Andalucía, IAA-CSIC, Glorieta de la Astronomía s/n, E-18008 Granada, Spain*
[5]*Department of Space, Earth, and Environment, Chalmers University of Technology, Onsala Space Observatory, SE-439 92 Onsala, Sweden*
[6]*Institute of Astronomy and Astrophysics, Academia Sinica (ASIAA), No. 1, Section 4, Roosevelt Road, Taipei 10617, Taiwan*
[7]*Instituto de Astronomía, Universidad Nacional Autonoma de México, Apdo. Postal 106, 22800 Ensenada, B.C., Mexico*

ABSTRACT

Born-again planetary nebulae (PNe) are extremely rare cases in the evolution of solar-like stars. It is commonly accepted that their central stars (CSPN) experienced a *very late thermal pulse* (VLTP), ejecting H-deficient material inside the evolved H-rich PN. Given the short duration of this event and the fast subsequent evolution of the CSPN, details of the mass ejection are unknown. We present the first morphokinematic model of the H-deficient material surrounding a born-again PN, namely A 30. New San Pedro Mártir observations with the Manchester Echelle Spectrograph were recently obtained to map the inner region of A 30 which are interpreted by means of the software SHAPE in conjunction with *HST* WFC3 images. The SHAPE morphokinematic model that best reproduces the observations is composed by a disrupted disc tilted 37° with respect to the line of sight and a pair of orthogonal opposite bipolar ejections. We confirm previous suggestions that the structures closer to the CSPN present the highest expansion velocities, that is, the disrupted disc expands faster than the farther bipolar features. We propose that the current physical structure and abundance discrepancy of the H-deficient clumps around the CSPN of A 30 can be explained by a common envelope phase following the VLTP event. Our proposed scenario is also compared with other known born-again PNe (A 58, A 78, HuBi 1, and the Sakurai's Object).

Key words: circumstellar matter – stars: evolution – stars: mass-loss – stars: winds, outflows – planetary nebulae: individual: PN A66 30.

1 INTRODUCTION

The planetary nebula (PN) Abell 30 (PN A66 30 or PN G 208.5+33.2; hereinafter A 30) is a H-deficient PN that is accepted to have experience a *born-again* event ≲900 yr ago (Fang et al. 2014). It exhibits a double-shell morphology that includes an outer H-rich almost spherical shell with a radius of ~1 arcmin and an inner H-deficient cloverleaf-like structure that extends ~30 arcsec from the central star (CSPN; Jacoby 1979).

The brightest H-deficient clumps are located ≲10 arcsec from the CSPN. Initial low-resolution optical images disclosed four main structures which were labelled as knot 1, 2, 3, and 4 (Jacoby 1979), but these have been demonstrated later to be a collection of smaller clumps and filaments through high-spatial resolution *Hubble Space Telescope* (*HST*) images (see Borkowski et al. 1993; Borkowski,

Harrington & Tsvetanov 1995, and Fig. 1). In the following, we will adopt the notation initially defined by Reay, Atherton & Taylor (1983) of J1, J2, J3, and J4 for the knots, which correspond to the structures located towards the SE, NE, NW, and SW from the CSPN of A 30, respectively. These are highlighted with green circles in Fig. 1.

There have been several spectroscopic studies of the H-deficient clumps in A 30 which suggest that there are noticeable differences between knots J1–J3 and those of J2–J4 (e.g. Jacoby & Ford 1983; Guerrero & Manchado 1996). The work of Simpson et al. (2022), in combination with results presented by Wesson, Liu & Barlow (2003), showed that there are also differences in the estimates of the abundance discrepancy factors (ADFs)[1] between knots. These works showed that the ADF for J4 is estimated to have an upper limit of 35, whilst that of J1 is estimated to be ~700. However,

---

★ E-mail: j.rodriguez@irya.unam.mx
† Visiting astronomer at Instituto de Astrofísica de Andalucía (IAA-CSIC, Spain) through the Centro de Excelencia Severo Ochoa Visiting-Incoming programme.

[1]The ADF is a widely-known problem in ionized nebulae originally reported by Wyse (1942) consisting in the discrepancy between the chemical abundances derived from recombination lines and collisionally excited lines. Typical values of the ADFs are around 2 (see Wesson et al. 2018).
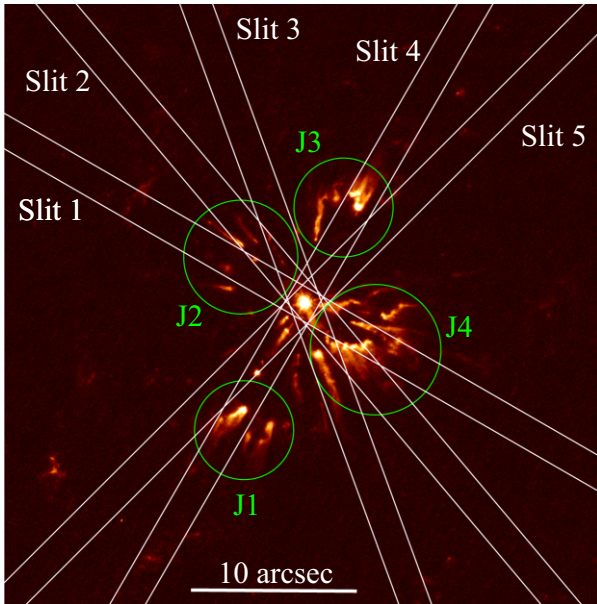
Figure 1. *HST* [O III] 5007 Å narrow-band image of the central region surrounding the CSPN of A 30. The position of the SPM MES slits are illustrated and labelled as Slits 1–5 (see details in Table 1). The green circles delineate the previously unresolved clumps defined as J1–J4 (Reay et al. 1983). North is up, east to the left.

Table 1. SPM MES observations of A 30. All spectra have exposure times of 1200 s and were taken through a filter that isolates the [O III] λ5007 Å emission line (see the text for details).

Slit	PA	Date	Seeing
	(°)	(yyyy mmm dd)	(arcsec)
1	60	2020 Jan 20	3.0
2	40	2020 Jan 20	3.0
3	20	2020 Jan 20	3.0
4	−30	2020 Jan 21	2.0
5	−45	2020 Jan 21	2.0

models including gas and dust to find that, after accounting for the C trapped in the dust, the C/O ratio of $\gtrsim 1$ is consistent with a single star experiencing a VLTP (see e.g. Miller Bertolami et al. 2006, and references therein).

In this paper, we present the first morphokinematic study of the inner H-deficient clumps in A 30 to assess the details of their ejection scenario and shaping. High-resolution SPM MES spectra were recently acquired and modelled with the use of the SHAPE software (Steffen et al. 2011).

The paper is organized as follows. In Section 2 we present our observations and data reduction. The interpretation of the high-resolution spectra through a morphokinematic model is presented in Section 3. Our results are discussed in Section 4 where we propose a shaping mechanisms of the H-deficient clumps. Finally, our conclusions are presented in Section 5.

2 OBSERVATIONS AND DATA PREPARATION

Long-slit high-dispersion optical spectra of A 30 were obtained using the MES mounted on the 2.1m telescope at the Observatorio Astronómico Nacional at San Pedro Mártir (OAN-SPM, Mexico).[2] The data were obtained on 2020 January 20 and 21 (see Table 1) using the E2V 42-40 CCD with a pixel size of 13.5 μm pix^{-1} and a 4 × 4 on chip binning, which resulted in a plate scale of 0.702 arcsec pix^{-1}. A series of spectra were taken with exposures of 1200 s through the [O III] 5007Å filter ($\Delta\lambda = 50$ Å) to isolate the 114th order (0.086 Å pix^{-1} spectral scale). The slit width of 150 μm (1.9 arcsec) leads to a spectral resolution of 12 ± 1 km s^{-1}.

We observed five slits positions across the CSPN of A 30 along different position angles (PAs) to cover most of the H-deficient clumps and filaments surrounding the CSPN. The slit positions are illustrated in Fig. 1 and the journal of observations is given in Table 1.

The spectra were processed using standard calibration routines in IRAF (Tody 1993), including bias subtraction and wavelength calibration with ThAr arc lamps obtained immediately before and after the science observations. The wavelength accuracy is estimated to be ± 1 km s^{-1}.

The resultant position–velocity (PV) diagrams[3] of the five spectra are presented in Fig. 2. These resemble PV diagrams previously presented by other authors, with an outer almost spherical shell extending ≈ 1 arcmin in radius and high-velocity structures ($\lesssim 200$ km s^{-1}) contained within the inner 30 arcsec (see Section 1). To highlight the

it appears that without the information of the H mass fraction in the different clumps one cannot make strong statements on possible abundance differences. Simpson et al. (2022) concluded that specific 3D photoionization modelling of A 30 is most needed in order to understand these differences.

To our knowledge, Dinerstein & Lester (1984) were the first to suggest the existence of a disc-like structure surrounding the CSPN of A 30. This structure, unveiled by near-IR observations, was suggested to be tracing knots J2 and J4 as later found by Borkowski et al. (1994). Subsequently, narrow-band images of the H-deficient clumps mainly, obtained through the [O III] 5007 Å filter, have been used to described them as part of a disrupted disc and a couple of bipolar ejections (Borkowski et al. 1993; Harrington 1996).

We note that there is no detailed morphokinematic study of A 30 in the literature, although several kinematic studies indeed support the expanding disc and jet structure (e.g. Reay et al. 1983; Jacoby & Chu 1989; Yadoumaru & Tamura 1994; Chu, Chang & Conway 1997). The study presented by Meaburn & Lopez (1996) disclosed a more detailed kinematics given the large number of spectra and the higher spectral resolution. These authors used San Pedro Mártir (SPM) Manchester Echelle Spectrograph (MES; Meaburn et al. 2003) observations to show that the radial expansion velocity of the outer H-rich nebula is 38.5 ± 1.0 km s^{-1}, while the H-poor material exhibits a range of velocities from ~40 to a few times 100 km s^{-1}.

The mass ejection from a single star cannot produce a bipolar morphology (e.g. García-Segura et al. 2014). Therefore, the bipolar structure of the H-deficient clumps in A 30 (disrupted disc + jet) has to be attributed to the action of a companion, either stellar or, as suggested a few decades ago by Soker (1997), substellar. Indeed A 30 possesses the highest ADF among PNe, a property strongly correlated with binarity (Wesson et al. 2018), and the brightness variation period of 1.06 d of its CSPN in *Kepler/K2* observations has been attributed to the presence of a companion (Jacoby, Hillwig & Jones 2020). Nevertheless, Toalá et al. (2021) used photoionization

---

[2]The Observatorio Astronómico Nacional at the Sierra de San Pedro Mártir (OAN-SPM) is operated by the Instituto de Astronomía of the Universidad Nacional Autónoma de México.

[3]The PV diagrams were produced with the matplotlib PYTHON routines developed by Hunter (2007).
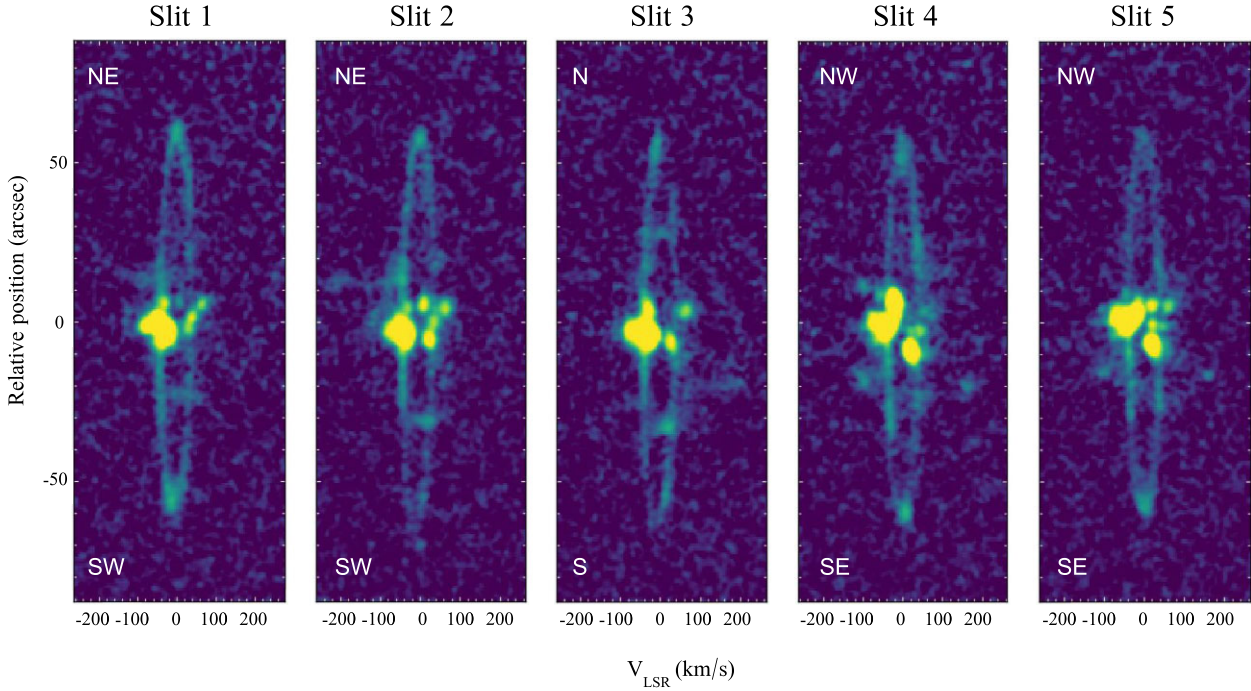
Figure 2. PV diagrams obtained from the SPM MESS [O III] spectra of A 30 for slits 1–5.

structures close to the CSPN of A 30, we show close-ups of the PV diagrams in Fig. 3-top.

3 MORPHOKINEMATIC MODEL

The software SHAPE was used to interpret the SPM MES [O III] spectra and *HST* WFC3 [O III] image of A 30. SHAPE allows the user to define different 3D geometric structures that can be edited (truncated, rotated, and stretched) in order to produce shapes that resemble those of the direct images of the studied objects. Moreover, expansion velocity laws can be defined for the different structures and, subsequently, synthetic PV diagrams can be produced and compared to those observed.

A simplistic model consistent of a toroidal structure and a pair of spherical clumps mimicking the jet-like features was first attempted. Not surprisingly, those structures did not produce images nor PV diagrams similar to the observed ones as the H-deficient clumps and filaments in A 30 are actually composed by collections of discrete knots. Furthermore, it was clear that the clumps and filaments in the so-called disrupted disc are not equidistant to the CSPN of A 30. To improve the model, tailor-made structures were defined for each individual clump. These consisted of truncated tori, i.e. structures with the appearance of a doughnut slice. Those corresponding to the disrupted disc were assumed to be distributed mostly along the same plane, that will be referred as the equatorial plane, whereas those of the jet-like features were assumed to be mostly along the orthogonal direction, i.e. the symmetry axis of the disrupted disc. The model further assumes that the symmetry axis of the disrupted disc and thus the jet-like features have a PA on the sky of $-30°$, the same used for slit 4 (see Table 1).

The shape of each individual structure and their velocities were then fine-tuned until the features in the synthetic [O III] image and PV diagrams were satisfactorily reproduced. Each truncated torus is defined by its distance to the star, thickness, length along the radial direction, and height over the equatorial plane. The velocity at each

point of these truncated tori is assumed to be radial and its modulus v is proportional to its radial distance r

$$v(r) = v_0 \left(\frac{r}{r_0} \right), \tag{1}$$

where r_0 is the distance from the facing-side of the clump to the CSPN and v_0 is a characteristic velocity of each clump. This velocity law thus includes a velocity gradient within each clump that takes into account the head to tail velocity difference in a cometary knot.

The best SHAPE model of A 30 is presented in Fig. 4 and the resultant synthetic PV diagrams are presented in the bottom panels of Fig. 3 in comparison with those observed. Edge- and pole-on projections of the best SHAPE model are also presented in the top-middle and top-right-hand panels of Fig. 4.

This model includes 20 more or less coplanar truncated tori around the CSPN illustrated in green in Fig. 4. These structures are located on a plane with an average inclination angle i of $37° \pm 4°$ with respect to the line of sight, they have distances from the CSPN of A 30 ranging between 2.1 and 11.4 arcsec, with an averaged distance of 8.3 arcsec, and the average disc expansion velocity has a value V_{disc} of 105 ± 5 km s^{-1}, where the errors on i and V_{disc} are derived empirically solely based on the accuracy in reproducing the observed PVs and image by the model. The model requires the brightest SW optical knots to be slightly larger (see Fig. 4). Interestingly, the characteristic velocity of each clump v_0 decreases with their distance to the CSPN, in agreement with the results obtained by Fang et al. (2014) based on their proper motions. These structures fairly reproduce the morphology and kinematics of the disrupted disc[4] as illustrated in the bottom panels of Figs 3 and 4.

Meanwhile the jet-like features are reproduced using two groups of truncated tori, with the farthest ones along a direction orthogonal

---

[4]We note that this comparison is limited by the lower spatial resolution of the kinematic data compared to the superb *HST* image quality.
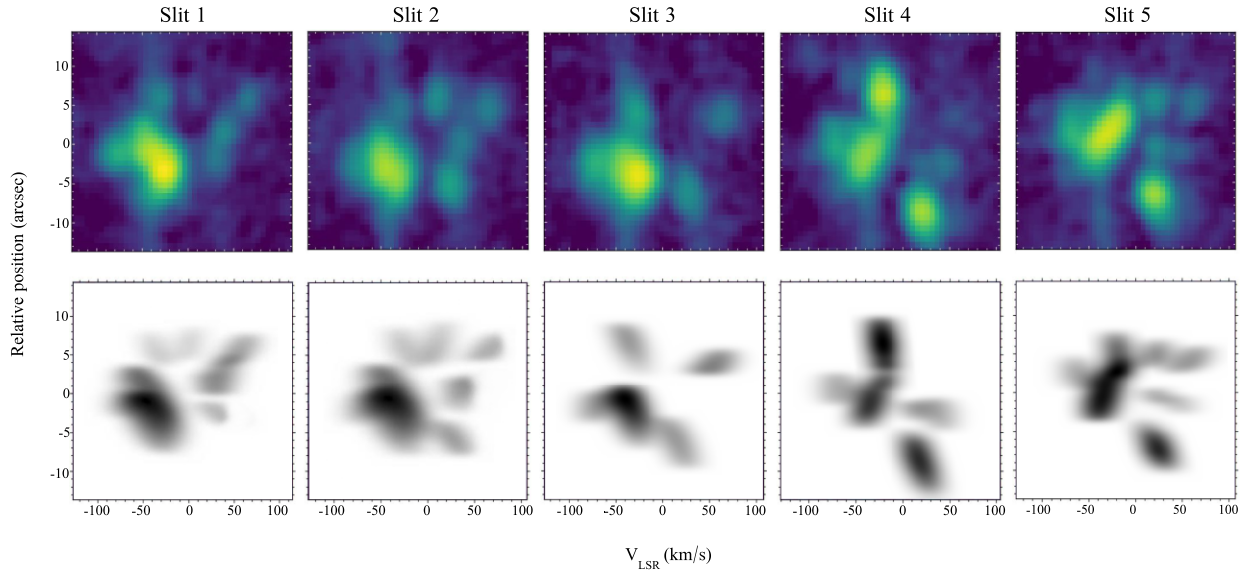
Figure 3. Top panels: PV diagrams obtained from the SPM MES [O III] spectra of the central region of A 30. Bottom panels: Synthetic PV diagrams obtained from our SHAPE model (see Section 3).
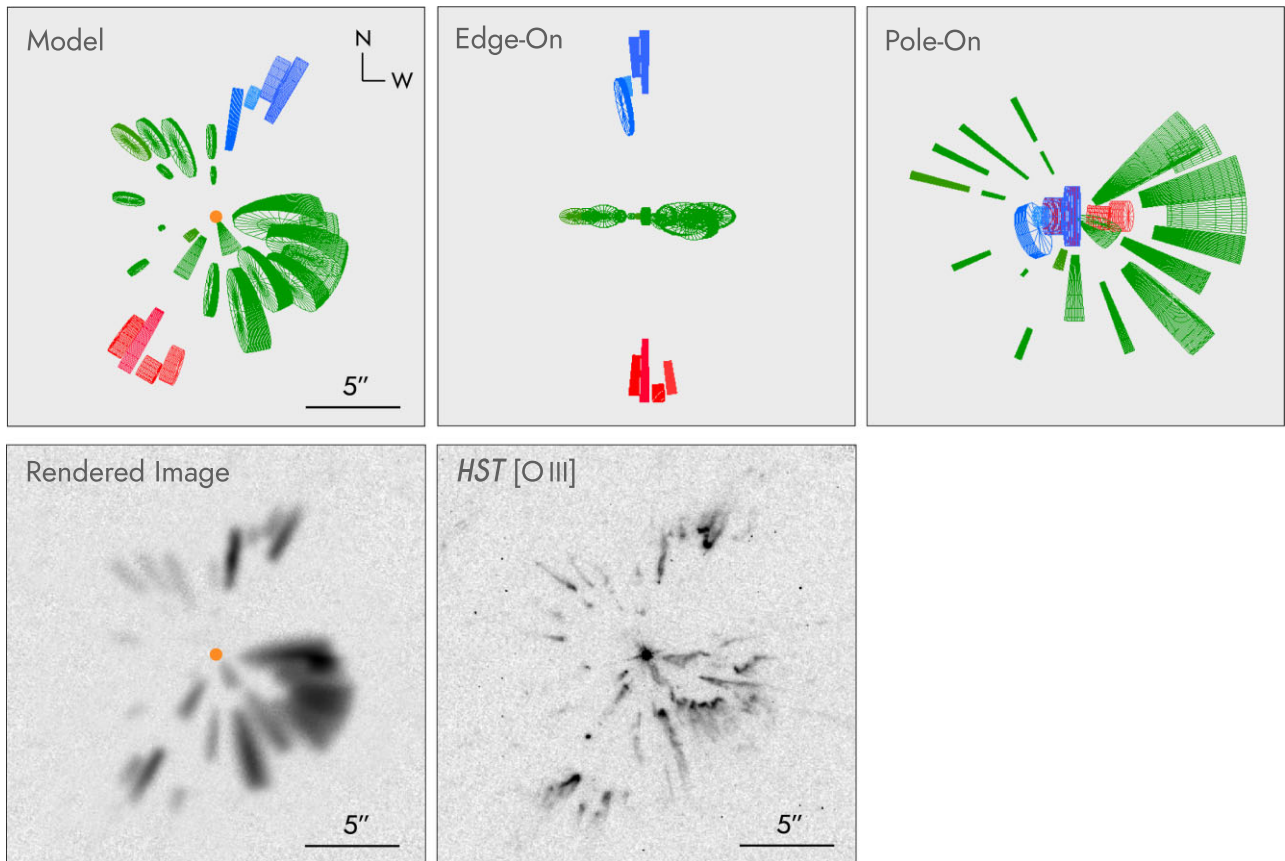

Figure 4. Morphokinematic model of A 30 obtained with the software SHAPE. Top panels show our best model through different viewing angles where features in green, blue, and red denote the disrupted disc and the approaching and receding jet-like structures in A 30, respectively (see Section 3 for details). The bottom left-hand panel shows a rendered image which is compared with the *HST* [O III] image in the bottom right-hand panel. The position of the CSPN is illustrated with an orange dot in the leftmost panels. The edge- and pole-on images do not have the same scale as the other panels, they are presented for illustrative purposes only.
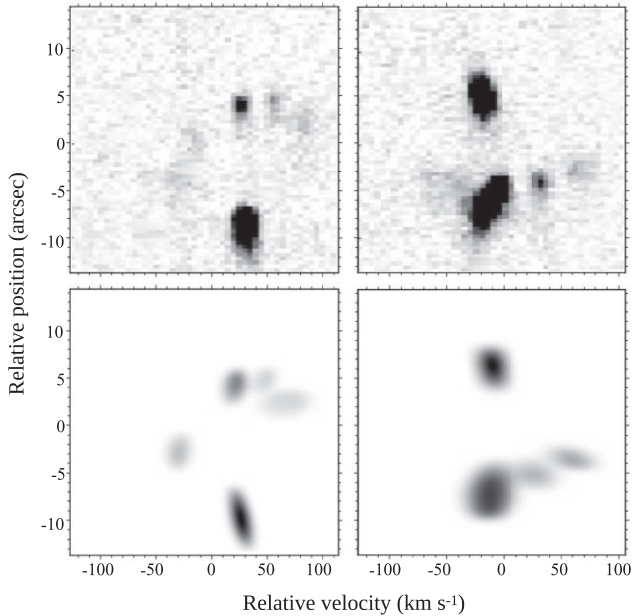
Figure 5. Top panels: High-dispersion [O III] spectra of A 30 presented in Chu et al. (1997) obtained at the 4 m Kitt Peak National Observatory. Bottom panels: Synthetic spectra obtained from our best SHAPE model of A 30. The spectra were obtained with a PA = 0° in a N-S direction passing through the SE polar knot (left-hand panels) and the NW polar knot (right-hand panels).

to that of the disrupted disc. These are located ∼24 arcsec from the CSPN and are illustrated in blue and red in Fig. 4 for the approaching and receding structures, respectively. As the jets are assumed to be orthogonal to the disrupted disc, the best-fitting model implies a deprojected expansion velocity for the jet clumps V_{jet} of 60 ± 5 km s^{-1} for the SE one and 45 ± 5 km s^{-1} for the NW one. The largest expansion velocity of the SE jet is also in agreement with its largest proper motion (Fang et al. 2014).

To further test our model, we also produced synthetic PV diagrams along long-slits similar to those presented by Chu et al. (1997). These were 1 arcsec wide and were oriented N-S at offsets 4 arcsec East and West of the CSPN of A 30, thus registering the SE and NW jet-like structures (knots J1 and J3), respectively, but also the eastern and western tips of the disrupted disc. The synthetic PV diagrams, shown in Fig. 5, exhibit very similar spatiokinematic patterns with those presented in fig. 4 of Chu et al. (1997).

4 DISCUSSION

Within the model limitations, the morphokinematic SHAPE model described above does an excellent job reproducing the observed PV diagrams and image of A 30 (see Figs 3 and 4). It definitely confirms that the H-deficient clumps surrounding the CSPN of A 30 are distributed on a disrupted disc and a pair of jet-like features.

Contrary to what would be expected from the kinematics of a disc and a bipolar jet produced at the same time during a thermonuclear explosion, our SHAPE model indicates that the clumps in the disc-like structure in A 30 expand faster than the jet features, while they are three times closer to the CSPN than those. These results are in line with those reported by Fang et al. (2014) who analysed multi-epoch *HST* WFPC2 and WFC3 images of A 30 and A 78 and showed that the proper motions of the H-deficient clumps in these two born-again PNe are higher for those closer to the CSPN. A number of different physical mechanisms such as photoionization, photoevaporation, the

rocket effect, and momentum transfer from the current fast wind to the dense clumps may have contributed altering the dynamics of the H-deficient ejecta and producing its complex morphology (see the discussion section in Fang et al. 2014).

The extreme bipolar morphology of the H-deficient clumps around the CSPN of A 30 seems to concur with the possible presence of a companion (Soker 1997; Jacoby et al. 2020), which can be invoked to explain the modulation of the mass-loss and the production of the disc + jet system. Nevertheless, the C/O ratio obtained after taking into account the C-rich dust in the ejecta in A 30 suggests a single-star VLTP event (Toalá et al. 2021). We propose that these apparently discrepant results can be simultaneously explained by invoking a VLTP followed by a common envelope (CE) evolution (Ivanova et al. 2013). This scenario, illustrated in Fig. 6, is detailed as follows:

(a) The CSPN of A 30 evolved from a binary system comprising an evolved WD (white dwarf) and a low-mass companion with masses M_1 and M_2, respectively (Fig. 6a).

(b) Following stellar evolution models, the WD experienced a VLTP causing the expansion of its outer layers and returning to the AGB locus of the HR diagram (see e.g. Iben et al. 1983, Fig. 6b). These predict a duration for the VLTP of decades to a few hundreds of years (see e.g. Miller Bertolami et al. 2006, and references therein).

(c) The radius increase of the primary caused the system to enter a CE phase (Fig. 6c). The companion transferred angular momentum to the envelope, producing a reduction of its gravitational binding energy. CE numerical simulations predict that this process reduces the orbital separation within time scales of months-to-years (see e.g. Chamandy et al. 2020). We refer to this stage as the CE-born-again (CEBA) phase.

(d) Numerical simulations have shown that the companion (M_2) can help shaping the mass-loss from the primary (M_1) during the CE phase. This process might have produced a toroidal structure followed by a subsequent bipolar ejection of material (see e.g. Zou et al. 2020; García-Segura, Taam & Ricker 2021; Lopez-Camara et al. 2021, and references therein). Thus, in A 30 the bipolar shaping took place during the duration of the VLTP. At this moment, the jet velocity V_{jet} was larger than the disc expansion velocity V_{disc} (Fig. 6d). As the ejecta in the bipolar component moved faster than the disc, it was located at larger distances from the CSPN than the toroidal structure. This phase will be referred as early born-again (EBA) phase.

(e) A large amount of works on born-again PNe suggests that the evolution of their CSPN is fast after experiencing a VLTP (see Evans et al. 2020; Hinkle et al. 2020, and references therein). The star shrinks and gets hotter so that a fast stellar wind and strong UV flux are developed. We propose that after the EBA phase, the increased stellar wind momentum and ionizing flux induced the toroidal structure to experience hydrodynamical instabilities that ultimately disrupted it into clumps and filaments within a few hundred years (see the simulations presented in Fang et al. 2014). The momentum transfer efficiency from the wind to the H-deficient material would be larger for closer structures. In particular, the CSPN of A 30, which experienced a VLTP about ≲900 yr ago, has a current stellar wind with a terminal velocity of ≈4000 km s^{-1} and an effective temperature of 115 kK (Guerrero et al. 2012). Accordingly, the clumps in the disc that were closer to the CSPN were accelerated faster than the bipolar structures, ultimately producing the current kinematic configuration where the jet velocity V_{jet} is smaller than the disc expansion velocity V_{disc} (Fig. 6e). We will refer to this stage as late born-again (LBA) phase and propose that A 30 can be actually placed into this evolutionary stage.
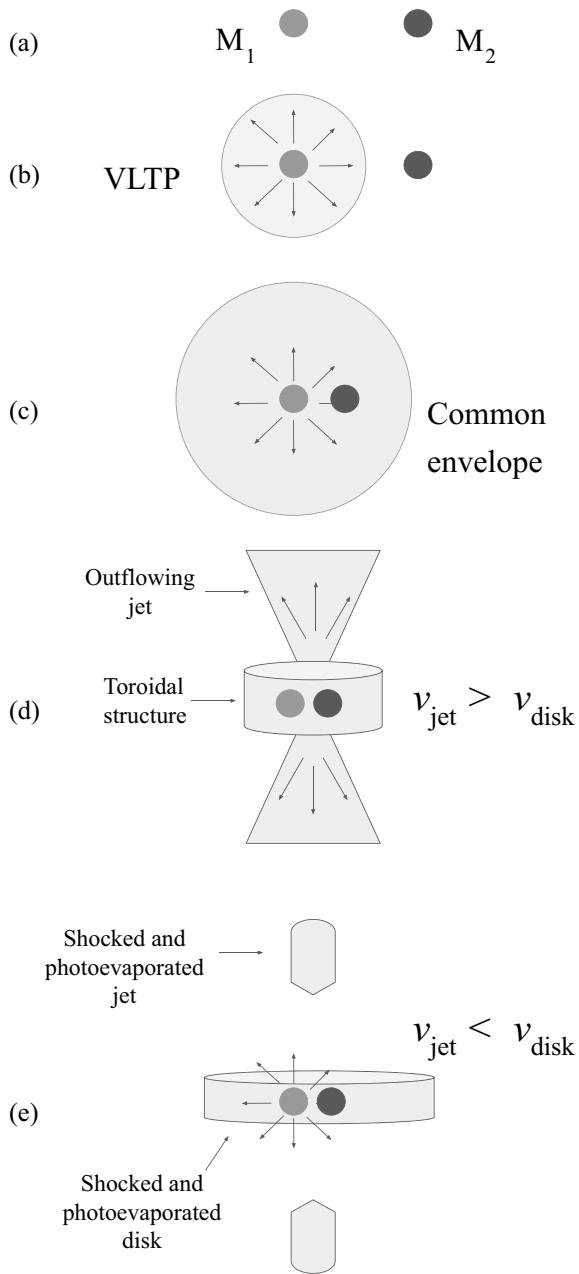
Figure 6. Cartoon of the evolutionary path of the H-deficient ejecta in A 30. This figure describes the CEBA scenario proposed in this work, in which a WD experiences a VLTP and the ejection of material is shaped into a bipolar morphology by a companion entering a CE phase. After the VLTP, the new WD develops a strong wind and ionizing photon flux that imprints momentum on to the H-deficient material. The closest structure is then accelerated faster than the bipolar structures. See Section 4 for details.

The proposed scenario can also help explaining the fact that the larger and brighter clumps and filaments in the disrupted disc of A 30 have a preferential distribution towards the SW of the CSPN. Simulations have shown that the toroidal structure formed as the result of a CE evolution is uneven and inhomogeneous (see for example, fig. 1 in Ondratschek et al. 2022, and their associated videos). Density enhancements appear and get diluted towards the equator of the toroidal structure in short time-scales and are not symmetric given the orbital motion of the companion star. Thus, it

is very likely that by the time the fast wind and the UV flux of the CSPN of A 30 increased, a density enhancement existed towards the SW.

In the proposed CEBA evolution scenario (see Fig. 6), the disc and jet abundances would be the same and thus we suggest that the differences in their ADFs reported by Simpson et al. (2022) should be rather attributed to their different physical properties. These would produce variations in the extent of the temperature (Peimbert 1967) and density fluctuations (Viegas & Clegg 1994), or in the clumping of the H-deficient material (Liu et al. 2000), which have long been suggested to cause the ADF (see e.g. Wesson et al. 2018, and references therein). The IR study of A 30 presented by Toalá et al. (2021) indeed points to different physical properties between the disc and jet, with dust at temperatures of $\lesssim 200$ K mainly present in the disrupted disc of A 30. Alternatively, the interaction of the companion with the expanded star envelope during the CEBA and EBA phases, which would feed the disc with processed material, may result in chemical abundances different for the jet and disc. As concluded by Simpson et al. (2022), it is critical to assess the specific mass fraction of H-poor and H-rich material of the different components of the ejecta to peer into this problem.

A detailed 2D mapping of the chemical abundances for each clump in A 30 would resolve this issue, and appropriate high-dispersion integral field spectroscopic data of A 30 are been currently sought. In addition, radiation-hydrodynamic numerical simulations following in detail the stellar evolution of stars experiencing a VLTP will be used in the future to test our proposed CEBA scenario and to assess the time-scales on the formation of the complex structures in born-again PNe (Rodríguez-González et al., in preparation).

4.1 Comparison with other born-again PNe

The proposed CEBA scenario can be used to describe the characteristics of other born-again PNe. In particular, we note that A 78 shares many similarities with A 30. The morphology of the dense H-deficient clumps in A 78 also resemble a disrupted disc + jet system and their expansion parallaxes and radial velocity patterns are very similar to those of A 30 (e.g. Meaburn et al. 1998), as well as their kinematic ages, $\lesssim 10^3$ yr (Fang et al. 2014). In addition, their CSPNe exhibit almost the same properties (see Toalá et al. 2015). Thus, it can be envisaged that the CEBA scenario proposed for A 30 would also explain the properties of A 78. A detailed morphokinematic model of A 78 is needed to fully confirm these suggestions.

The born-again PN A 58, which experienced its VLTP in 1919, about 100 yr ago, also displays a bipolar ejection with a dense toroidal structure almost obscuring its CSPN (Hinkle et al. 2008). The expansion velocity of the optical ejecta has been shown to be ~ 200 km s^{-1} (Clayton et al. 2013), but recent ALMA observations of the molecular component of A 58 demonstrated that the toroidal structure expands with a velocity of 90 km s^{-1} from the CSPN whilst the bipolar emission has a faster velocity of 280 km s^{-1} (Tafoya et al. 2022). Interestingly, these authors found that the molecular material in the bipolar ejection can be traced closely to the CSPN and has a kinematic age of $\lesssim 20$ yr, i.e. apparently younger than the VLTP event. The effects of the fast stellar wind and strong UV flux from the CSPN of A 58 are not yet dominant as in A 30 and A 78. Thus, under our proposed scenario, A 58 can be placed in the EBA phase of the evolution of a VLTP ejecta (Fig. 6d).

The youngest born-again PN, the Sakurai's Object, experienced its VLTP event in 1996 February, about 26 yr ago. Only two years later, in 1998 March, material expanding at velocities up to -550 km s^{-1} was revealed by a blue-shifted absorption line of He I

10830 (Eyres et al. 1999). Soon afterwards, optical observations obtained on 2001 detected a bipolar outflow in the [N II] emission lines with two components at systemic velocities of -350 ± 50 and $+200 \pm 50$ km s^{-1} (Kerber et al. 2002), thus implying an average velocity close to the 290 km s^{-1} derived from the fundamental vibration-rotation CO band lines around 4.7 μm detected by Eyres et al. (2004) in 2003. This expansion velocity seems to have remained unchanged in the last decade (Hinkle & Joyce 2014; Hinkle et al. 2020). Subsequent modelling of the IR emission led Chesneau et al. (2009) to suggest the presence of a disc-like structure seen almost edge on, obscuring the progenitor star. Interestingly, the expansion velocity of the densest molecular material probed by the sub-mm detection of the HCN molecule is $\gtrsim 100$ km s^{-1} (Tafoya et al. 2017). If we assume that the densest molecular material is associated with the toroidal structure, its expansion velocity would be several times smaller than that of the bipolar outflow. This would place Sakurai's Object in the EBA phase, where the bipolar ejection is still faster than the disc-like structure. Our team has gathered ALMA data to map the molecular and continuum emission of Sakurai's Object to probe the extreme bipolar morphology of this born-again PN (Tafoya et al., in preparation).

The last addition to the born-again PN class is HuBi 1 (Guerrero et al. 2018; Montoro-Molina et al. 2022). The 2D spatiokinematic properties of its H-poor ejecta have been interpreted as a prolate ellipsoidal shell (Rechy-García et al. 2020), although the extremely bright emission around the systemic velocity and weakness of the fastest components suggests an alternative physical model consistent of a bright equatorial disc mostly on the plane of the sky and a bipolar outflow tilted with the line of sight. The similarity between the expansion velocity of the disc on the plane of the sky[5] of 290 km s^{-1} and that of the bipolar outflows of 250 km s^{-1} (Rechy-García et al. 2020) suggests that HuBi 1 would be in the transition between the EBA and LBA phases. Indeed HuBi 1 experienced its VLTP about 200 yr ago (Rechy-García et al. 2020) and thus it has an intermediate age between A 58 and the more evolved A 30 and A 78.

4.2 Model caveats

The proposed morphokinematic model and CEBA scenario provide a reasonable description of the morphology and spatiokinematics of A 30 and its formation and evolution. Still we would like to mention a few caveats.

The availability of a throughout investigation of the proper motion of the knots of A 30 using multi-epoch *HST* WFPC2 and WFC3 images (Fang et al. 2014) allows investigating their tangential velocity and thus their inclination in conjunction with the observed radial velocities. Unfortunately, the knots of the disrupted disc are not well resolved in our morphokinematic data and they cannot be assigned to the corresponding knot resolved in the *HST* images. This investigation is still viable for the polar knots. The proper motions of NW (J3) and SE (J1) clumps is reported to be 7.93 and 6.99 mas yr^{-1}, respectively. At the updated distance to A 30 of 2.08 ± 0.14 kpc (Bailer-Jones et al. 2021), this implies tangential velocities of 69 km s^{-1} for the NW jet (J3) and 78 km s^{-1} for the SE jet (J1). The observed averaged systemic radial velocities of these jets are -15 ± 5 km s^{-1} and $+21 \pm 5$ km s^{-1}, respectively, where the error is introduced to account for their velocity gradient in the PV maps. The tangential and radial velocities imply expansion velocities and inclinations with the plane of the sky of 71 ± 2 km s^{-1}

and $12° \pm 4°$ for the NW jet, and 81 ± 2 km s^{-1} and $15° \pm 4°$ for the SE jet. These results indicate that the SE jet moves faster than the NW jet, as in the morphokinematic model presented Section 3, but, unlike in the model, the polar outflows are not orthogonal to the disrupted disc, which would require an inclination of 37°. This is not a major issue, as the inclination of the polar outflow in the model is an independent parameter that can be fine-tuned together with the expansion velocity of the outflow. Interestingly, the bipolar ejection in Sakurai's Object is neither orthogonal to its equatorial disc (see fig. 2 in Hinkle et al. 2020). We note that the field of study of jet evolution and effects during the CE phase is very active, with simulations showing deviations from a linear motion and choking effects in jets (see e.g. Zou et al. 2022, and references therein) that are not taken into account in the proposed CEBA scenario.

The comparison of the different born-again PNe in the previous section has evidenced that the H-poor ejecta in all of them can be interpreted as the combination of a disc and a jet. Their expansion velocities, however, are very different from one born-again PN to another. The discs and jets of A 30 and A 78 exhibit much lower expansion velocities than those of the Sakurai's Object, A 58 and HuBi 1, event though the current fast stellar wind from their CSPNe are imprinting momentum to the H-deficient clumps. It shall be noticed that, in the CEBA scenario, the bipolar ejection is produced by the presence of a companion. At early times, the velocity of the bipolar ejection is more or less the escape velocity

$$v_{\text{esc}} = \sqrt{2G\frac{M}{R}}, \tag{2}$$

associated to the companion producing the jet, whereas the expansion velocity of the disc would depend both on the mass of the companion and its final orbital radius. There are no estimations of the mass and/or spectral types of the companions of the CSPN of born-again PNe, neither of their orbital radii, but it can be easily envisaged that a variety of those can produce very different initial values of the disc and jet velocities in born-again PNe that would explain the large difference of observed expansion velocities. On the other hand, the released energy of the VLTP might not be the same for all born-again PNe, but we note that this idea seems more difficult to assess without modern stellar evolutionary models.

5 CONCLUSIONS

We presented the first morphokinematic model of the H-deficient ejecta in a born-again PN, namely A 30. We obtained SPM MES long-slit high-dispersion observations in the emission line of [O III] of the central H-deficient clumps that mapped the so-called disrupted disc and jets surrounding the CSPN of A 30. The observations were interpreted in conjunction with an *HST* WFC3 [O III] image of A 30 by means of the software SHAPE, which allowed us to produce a 3D model of the spatial distribution of the H-deficient ejecta and their expansion velocities.

Our best SHAPE model is able to explain the features unveiled by the [O III] PV diagrams and direct image. To reproduce the spatiokinematic signatures of the disrupted disc-like structure in A 30, our model requires the presence of a collection of clumps located mostly on a plane tilted by $37° \pm 4°$ with respect to the line of sight with averaged distance of 8.3 arcsec from the CSPN and a deprojected expansion velocity V_{disc} of 105 ± 5 km s^{-1}. The jet-like features are modelled by a pair of groups of clumps aligned mostly orthogonally with the disrupted disc. These expand with velocities V_{jet} of 45 ± 5 km s^{-1} for the approaching NW component and 60 ± 5 km s^{-1} for the receding SE one. The combination of the

---

[5]We note that this value depends on the rather uncertain distance to HuBi 1.

tangential and radial velocities of these jet components provides expansion velocities and inclinations with the plane of the sky of 71 ± 2 km s^{-1} and $12° \pm 4°$ for the NW jet, and 81 ± 2 km s^{-1} and $15° \pm 4°$ for the SE jet. This would imply that the bipolar outflow is not orthogonal to the disc, but this assumption on the morphokinematic model can be relieved just adopting expansion velocities and inclinations similar to those reported above. Together with the reports on the larger proper motions of the clumps located closer to the CSPN (Fang et al. 2014), the results above suggest that the jets and the disrupted disc in A 30 are apparently not coeval. Actually, they rather imply that their kinematics have been strongly affected by dynamical processes, which can be dominated by their photoevaporation and the transfer of momentum of the stellar wind.

We propose that the jets of A 30 have been produced during a CE phase between its CSPN and a companion. When the CSPN of A 30 experienced the VLTP, it might have inflated its outer layers causing a CE phase. The subsequent fast evolution of the CSPN of A 30 after the born-again event produced the current high ionization photon flux and fast stellar wind, which affects more strongly to the structure close to the CSPN, i.e. the disc. We suggest that whereas the kinematic properties of the jet-like features are currently similar to those during the CE phase, the clumps in the disc have experienced a strong acceleration caused by the fast stellar wind.

We propose that other born-again PNe can also be explained by the proposed CEBA scenario presented here. In particular, we suggest that A 30 and A 78 are at the same late stage of evolution, when wind momentum is efficiently transferred to the clumps in the disc and $v_{\rm jet} < v_{\rm disc}$. The younger born-again PNe A 58 and Sakurai's Object are arguably at a previous stage, when their CSPNe have not developed a strong stellar wind nor a strong UV flux to imprint momentum into the H-deficient material so that $v_{\rm jet} > v_{\rm disc}$. HuBi 1 would be in the transition between these two phases, with $v_{\rm jet} \simeq v_{\rm disc}$.

Future 3D radiation-hydrodynamic simulations following in detail the evolution of born-again scenarios in combination with a CE phase are needed to test the predictions presented here. High-dispersion integral field spectroscopic observations of A 30 and A 78 are sought to produce a 2D map of the ADF and C/O abundances among the different components of the H-poor ejecta. The availability of the proper motions of the clumps in these two born-again PNe on the plane of the sky (Fang et al. 2014) provides the unique opportunity to determine the inclination with the line of sight and true space velocity of each knot without any geometrical assumption to produce the first completely unbiased 3D model of the ejecta of born-again PNe.

DATA AVAILABILITY

The data underlying this article will be shared on reasonable request to the corresponding author.

REFERENCES

Bailer-Jones C. A. L. et al., 2021, AJ, 161, 147
Borkowski K. J. et al., 1993, ApJ, 415, L47
Borkowski K. J. et al., 1994, ApJ, 435, 722
Borkowski K. J., Harrington J. P., Tsvetanov Z. I., 1995, ApJ, 449, L143
Chamandy L. et al., 2020, MNRAS, 495, 4028
Chesneau O. et al., 2009, A&A, 493, L17
Chu Y.-H., Chang T. H., Conway G. M., 1997, ApJ, 482, 891
Clayton G. C. et al., 2013, ApJ, 771, 130
Dinerstein H. L., Lester D. F., 1984, ApJ, 281, 702
Evans A. et al., 2020, MNRAS, 493, 1277
Eyres S. P. S., Smalley B., Geballe T. R., Evans A., Asplund M., Tyne V. H., 1999, MNRAS, 307, L11
Eyres S. P. S., Geballe T. R., Tyne V. H., Evans A., Smalley B., Worters H. L., 2004, MNRAS, 350, L9
Fang X. et al., 2014, ApJ, 797, 100
García-Segura G. et al., 2014, ApJ, 783, 74
García-Segura G., Taam R. E., Ricker P. M., 2021, ApJ, 914, 111
Guerrero M. A., Manchado A., 1996, ApJ, 472, 711
Guerrero M. A. et al., 2012, ApJ, 755, 129
Guerrero M. A. et al., 2018, Nat. Astron., 2, 784
Harrington J. P., 1996, in Jeffery C. S., Heber U., eds, ASP Conf. Ser. Vol. 96, Hydrogen Deficient Stars. Astron. Soc. Pac., San Francisco, p. 193
Hinkle K. H., Joyce R. R., 2014, ApJ, 785, 146
Hinkle K. H. et al., 2008, A&A, 479, 817
Hinkle K. H. et al., 2020, ApJ, 904, 34
Hunter J. D., 2007, Comput. Sci. Eng., 9, 90
Iben I. et al., 1983, ApJ, 264, 605
Ivanova N. et al., 2013, A&AR, 21, 59
Jacoby G. H., 1979, PASP, 91, 754
Jacoby G. H., Chu Y.-H., 1989, Planet. Nebulae, 131, 183
Jacoby G. H., Ford H. C., 1983, ApJ, 266, 298
Jacoby G. H., Hillwig T. C., Jones D., 2020, MNRAS, 498, L114
Kerber F. et al., 2002, ApJ, 581, L39
Liu X.-W. et al., 2000, MNRAS, 312, 585
López-Cámara D., et al., 2021, preprint (arXiv:2110.02227)
Meaburn J., Lopez J. A., 1996, ApJ, 472, L45
Meaburn J. et al., 1998, A&A, 334, 670
Meaburn J. et al., 2003, Rev. Mex. Astron. Astrofis., 39, 185
Miller Bertolami M. M. et al., 2006, A&A, 449, 313
Montoro-Molina B., Guerrero M. A., Pérez-Díaz B., Toalá J. A., Cazzoli S., Miller Bertolami M. M., Morisset C., 2022, MNRAS, 512, 4003
Ondratschek P. A. et al., 2022, A&A, 660, L8
Peimbert M., 1967, ApJ, 150, 825
Reay N. K., Atherton P. D., Taylor K., 1983, MNRAS, 203, 1079
Rechy-García J. S. et al., 2020, ApJ, 903, L4
Simpson J. et al., 2022, Res. Notes Am. Astron. Soc., 6, 4
Soker N., 1997, ApJS, 112, 487
Steffen W. et al., 2011, IEEE Trans. Visual. Comput. Graph., 17, 454

Tafoya D. et al., 2017, A&A, 600, A23
Tafoya D. et al., 2022, ApJ, 925, L4
Toalá J. A. et al., 2015, ApJ, 799, 67
Toalá J. A. et al., 2021, MNRAS, 503, 1543
Tody D., 1993, in Hanisch R. J., Brissenden R. J. V., Barnes J., eds, ASP
    Conf. Ser. Vol. 52, Astronomical Data Analysis Software and Systems II.
    Astron. Soc. Pac., San Francisco, p. 173
Viegas S. M., Clegg R. E. S., 1994, MNRAS, 271, 993
Wesson R., Liu X.-W., Barlow M. J., 2003, MNRAS, 340, 253

Wesson R. et al., 2018, MNRAS, 480, 4589
Wyse A. B., 1942, ApJ, 95, 356
Yadoumaru Y., Tamura S., 1994, PASP, 106, 165
Zou Y. et al., 2020, MNRAS, 497, 2855
Zou Y. et al., 2022, preprint (arXiv:2202.05715)

This paper has been typeset from a TEX/LATEX file prepared by the author.